RADIATION BUDGET AND LONGWAVE CLOUD FORCING ANOMALIES FROM NOAA OPERATIONAL DATA

Arnold Gruber
NOAA/NESDIS & U.S. Naval Academy
Washington D. C. & Annapolis, Md., U. S. A.

1. INTRODUCTION

Estimates of the planetary radiation budget, albedo and outgoing longwave radiation, have been produced from the NOAA operational satellite system since June 1974. These estimates are obtained from high resolution cross track scanning radiometers, from observations in the visible (0.5-0.7 μm) and infrared window (10.5- 12.5 μm) portion of the spectrum. There are several issues related to the utility of this data set for the study of climate, especially since there are many simplifying assumptions and models and models applied to the estimation of broadband fluxes. Among the most important concerns are the accuracy and stability of the data set, which in turn affect its usefulness. After a brief review of how the data sets were derived the results of comparisons to collocated ERBE data will be presented and finally an analysis of longwave cloud forcing anomalies will be presented.

2. DETERMINATION OF RADIATION BUDGET PARMETERS

2.1 Albedo

The albedo is determined from the visible channel radiances by assuming that the reflected intensity is isotropic, that there is no solar zenith angle dependency and that the narrowband albedo is equal to the broad band albedo. This leads to an estimate of the albedo given by;

$$A = \pi N/(RS_f COS(z)) \quad (1)$$

where A is the albedo, N the reflected intensity, S_f the solar constant filtered by the response of the radiometer, R a correction for the mean earth sun distance and z is the solar zenith angle (Gruber, 1977). Subsequent work has highlighted the deficiencies in this "model"; e.g. Nimbus 7 bi-directional and solar zenith dependency models (Taylor and Stowe, 1984), and the applicability of visible narrowband albedo for different surfaces, (Laszlo, Jacobowitz and Gruber, 1988). The accuracy of the estimates are further compromised by the changes in the spectral response of the visible channel as new satellites were launched (Figure 1) and the lack of on board calibration as demonstrated by Staylor (1990) and Brest and Rossow (1990), who documented the degradation of the NOAA 9 visible channel. Nevertheless, as I shall show later the monthly mean fields exhibit a high degree of fidelity with broadband albedo measurements as obtained from ERBE.

In May 1988 the operational procedures for estimating the albedo were changed by including channel 2 (0.7 -1.1 μm) to estimate the broadband flux and by applying bi-directional and directional models to the estimates (Taylor, 1990). There still remains the problem of sensor degradation.

The data are archived in 2 formats; a 125 x 125 grid with a spatial scale that varies from about 100 - 200 km and a 2.5° latitude and longitude grid.

2.2 Outgoing longwave radiation (OLR)

The retrieval of the outgoing longwave radiation from a window channel measurements is based on a better foundation, both theoretical and empirical. The model used has evolved over time from a linear regression between window channel radiance and OLR calculated from simulations (Gruber, 1977) to a non linear model (Abel and Gruber, 1979) to the current empirical model. The model currently used is of the same form developed by Abel and Gruber except it is based on an empirical regression between co-located THIR and OLR

NORMALIZED RESPONSE FUNCTIONS

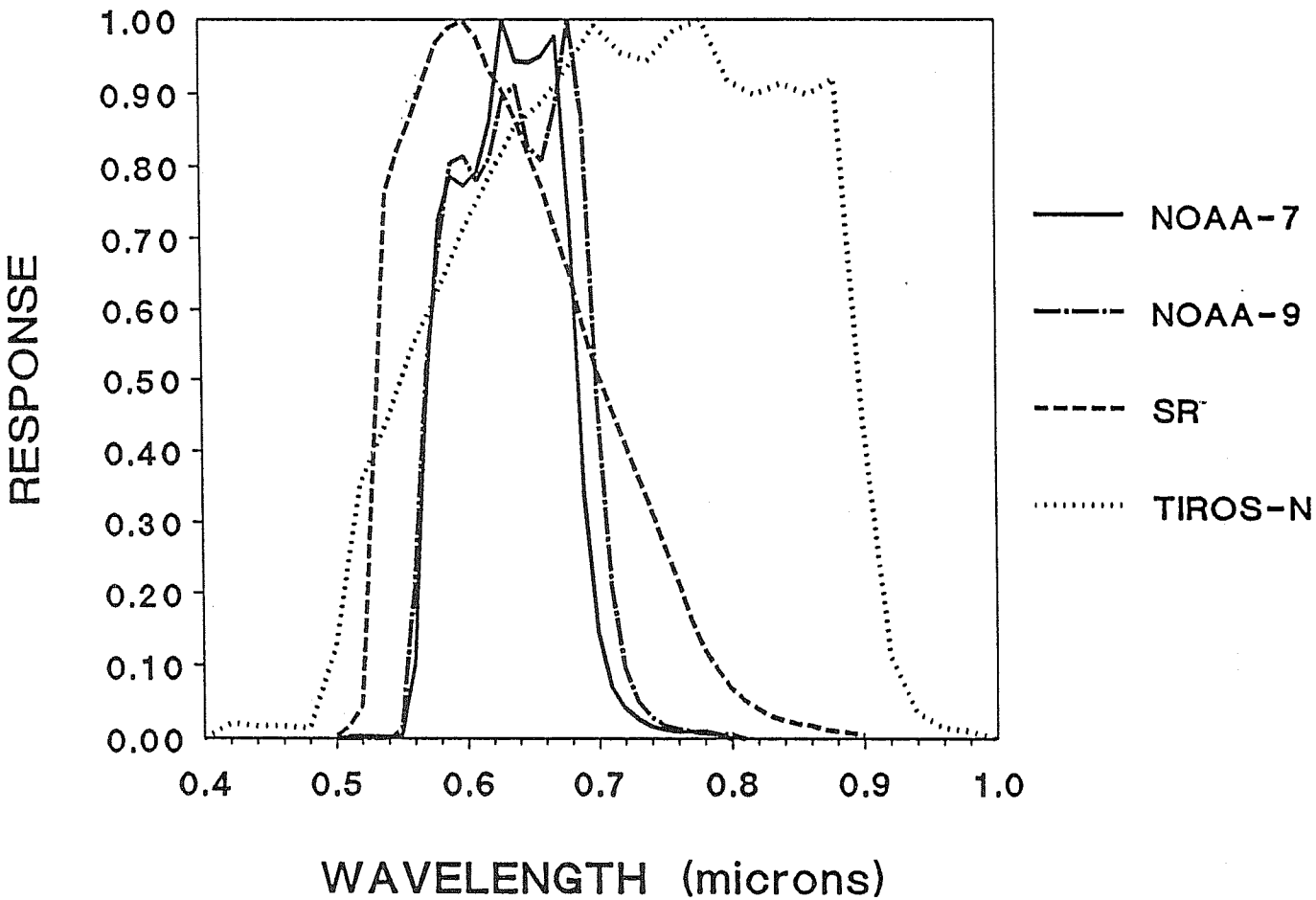

Fig. 1 Normalized response functions of the visible channels for TIROS-N, NOAA 7, 9 and SR (the radiometer prior to the TIROS-N series of satellites).

measurements from the Nimbus 7 Earth radiation budget experiment, (Ohring, Gruber and Ellingson, 1984). Adjustments are made for the different spectral responses of the NOAA radiometers and the THIR window channel (Gruber and Krueger, 1984). The actual form of the algorithm relates the limb darkened window brightness temperature to an equivalent flux temperature which is then used to calculate the flux (Eq. 2).

$$T_f = (a + bT_w)\,T_w$$
$$F = \sigma T_f^4 \qquad (2)$$

T_w is the window brightness temperature, T_f is the equivalent flux temperature, a, b are regression coefficients, F the OLR and σ the Stefan - Boltzman constant.

The OLR data are archived at the same scale as the albedo data.

3. COMPARISON WITH ERBE RESULTS.

The Earth Radiation Budget Experiment (ERBE),(Barkstrom, 1984) is designed to measure the planetary radiation budget with broadband instruments on 2 NOAA operational satellites and one dedicated research satellite. The instrument package consists of wide field (whole Earth disk) and medium field of view nadir pointing radiometers and a narrow field of view (≈ 50 km) scanning radiometer. The ERBE scanner has 3 channels: a shortwave (0.2-5 μm), a longwave (5 -50 μm) and a total channel (0.2-50 μm). Data from this radiometer are processed to provide flux values on a 2.5^0 latitude / longitude grid.

The presence of this instrument on the NOAA 9 operational spacecraft provided an excellent opportunity to validate the fluxes calculated from the narrowband scanning radiometers against collocated and coincident broadband measurements at the same spatial scale.

Comparisons were performed for April, July, October 1985, and January 1986. In collecting a compatible space and time

data set care was taken to insure that both ERBE and AVHRR data were present for a particular grid and time. If one of the grid boxes had missing data the other was not used.

3.1 Albedo comparisons

The daily and mean monthly ERBE albedo have angular models applied to them so this initial comparison does not separate the effects of narrowband estimates, bi-directional and directional models on the AVHRR shortwave estimates. Also no adjustments have been made to the AVHRR data for the sensor degradations mentioned previously. Nevertheless, the comparisons are informative. Figure 2 shows the global average mean and RMS difference of the reflected shortwave flux. The bias (ERBE > AVHRR) is 5 - 10 Wm^{-2} and the RMS ranges from 9 - 14 Wm^{-2}. This bias is present at all latitudes except in polar regions, as shown in Figure 3, which is the ratio of AVHRR to ERBE flux. The spatial distribution of the reflected energy for ERBE and AVHRR is shown for July in Figure 4 a,b. The spatial fidelity between the two data sets is clearly shown, e.g., the highly reflective cloudy areas in the tropics, the decrease (increase) of reflected energy with latitude in the winter (summer) hemisphere and the relatively low flux values over the subtropical oceans, which usually exhibit low clouds and thus low albedos. The difference is shown in Figure 5 and clearly exhibits the nearly uniform extent of the positive bias outside the polar region. Note that the clear land areas exhibit some of the largest differences, which is consistent with the fact that the visible albedo underestimates the albedo of vegetated land. The clear ocean and cloudy areas tend to show smaller but still positive differences. The correlation between the data sets is a surprisingly high .98, a further manifestation of the fidelity between them. The other months studied exhibit similar characteristics, including high correlations.

One should not be mislead by the statistical agreement however, since there may be compensating processes at work. For example, visible narrowband albedos are generally higher

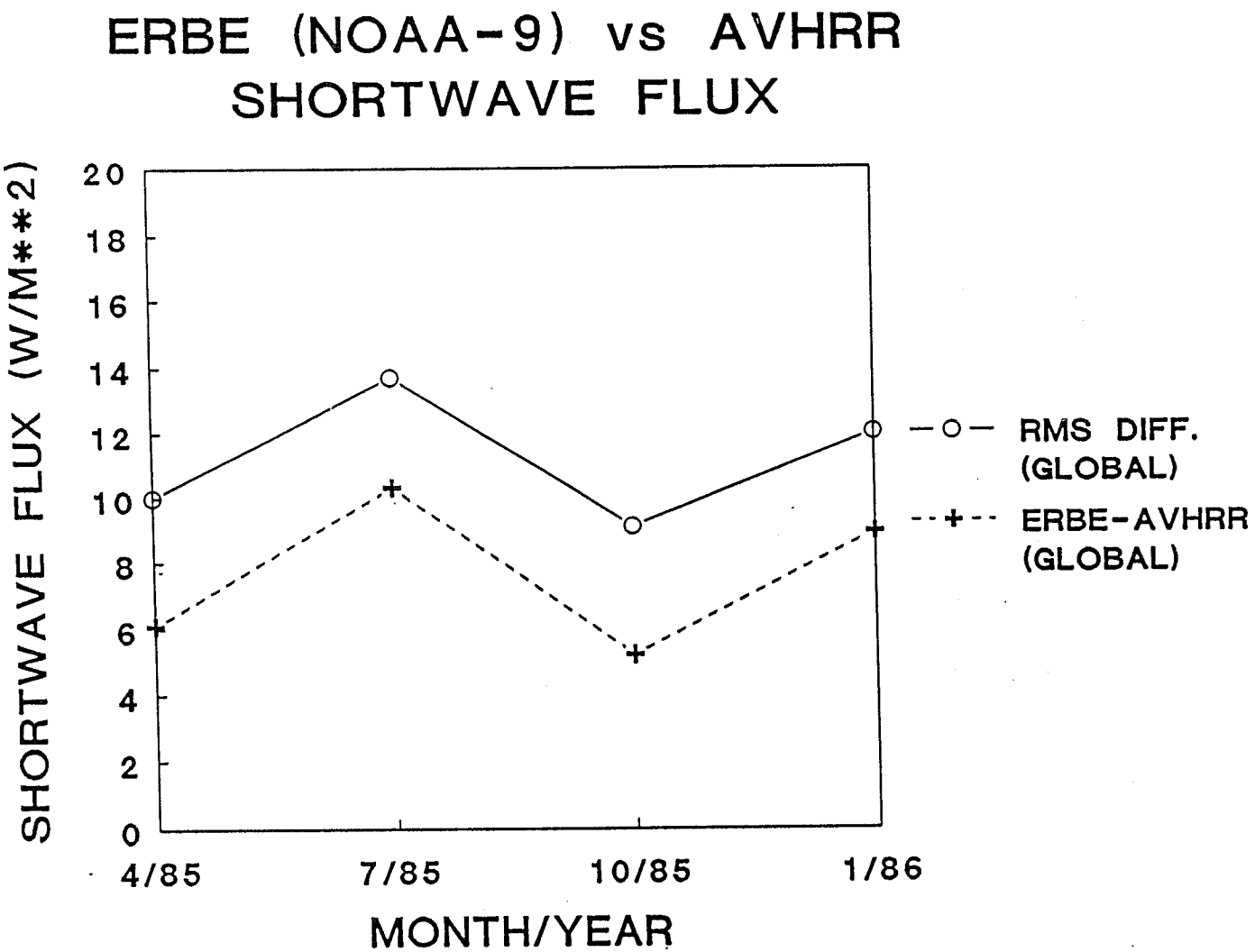

Fig. 2 Shortwave mean and RMS difference (ERBE-AVHRR) in Wm^{-2} for April, July, October, 1985 and January 1986.

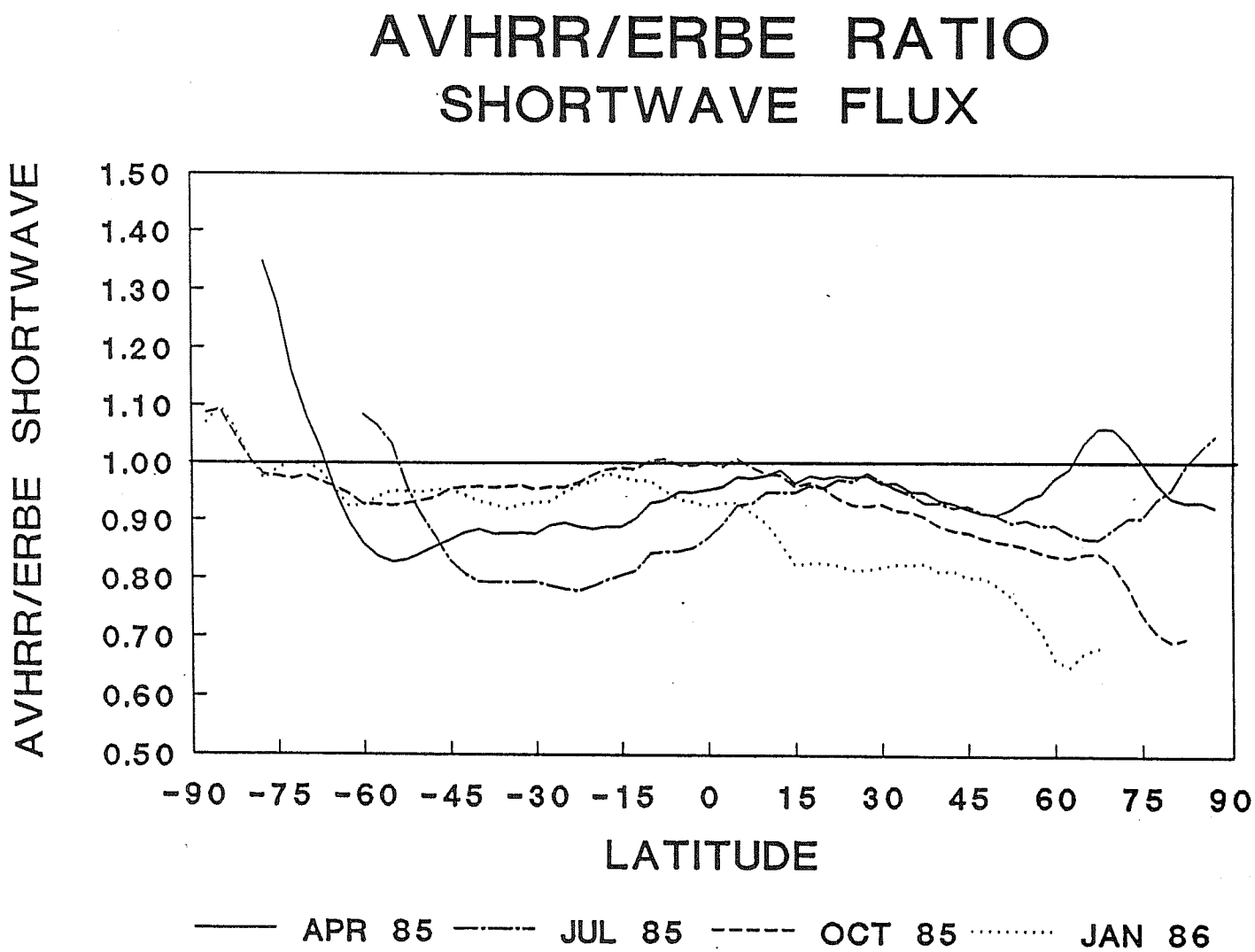

Fig. 3 Ratio of zonal average AVHRR to ERBE shortwave flux illustrating that the bias is present at nearly all latitudes.

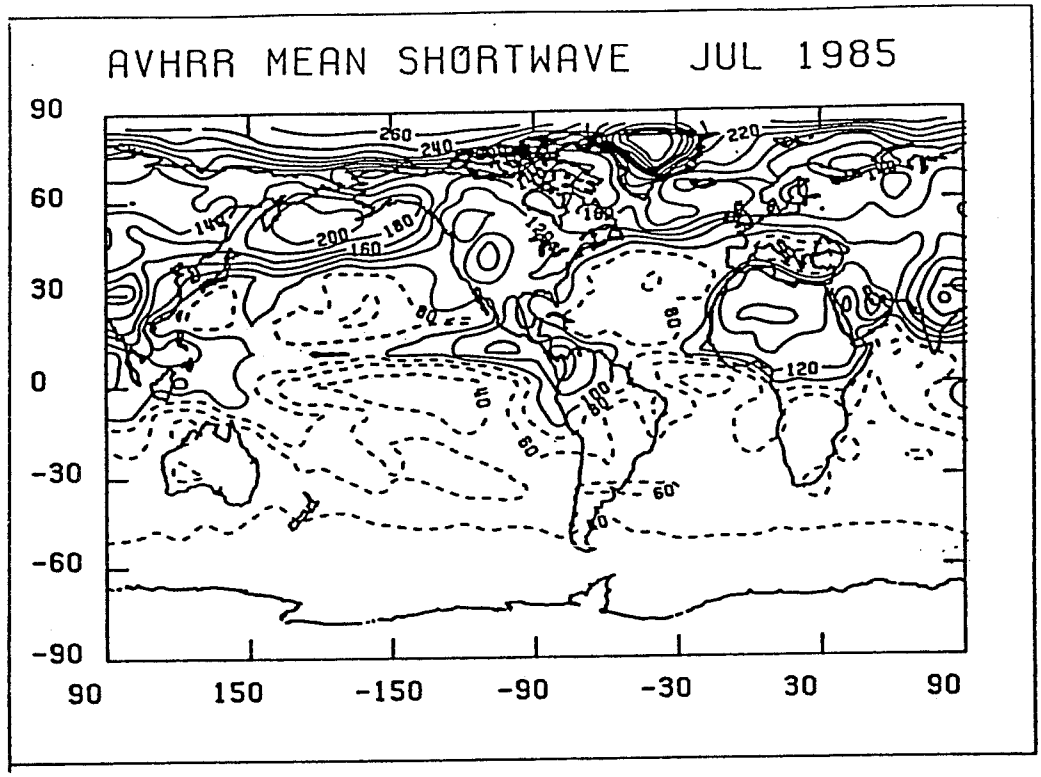

(a)

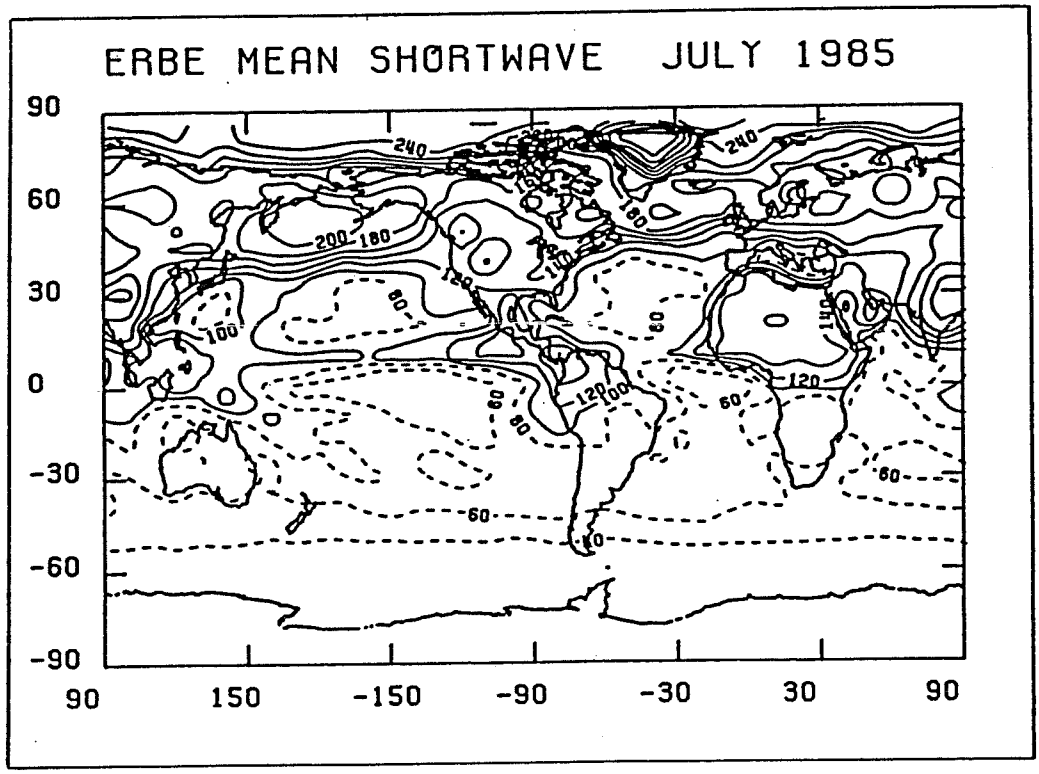

(b)

Fig. 4 Spatial distribution of shortwave flux, Wm^{-2}, (a) AVHRR (top), (b) ERBE (bottom), July 1985.

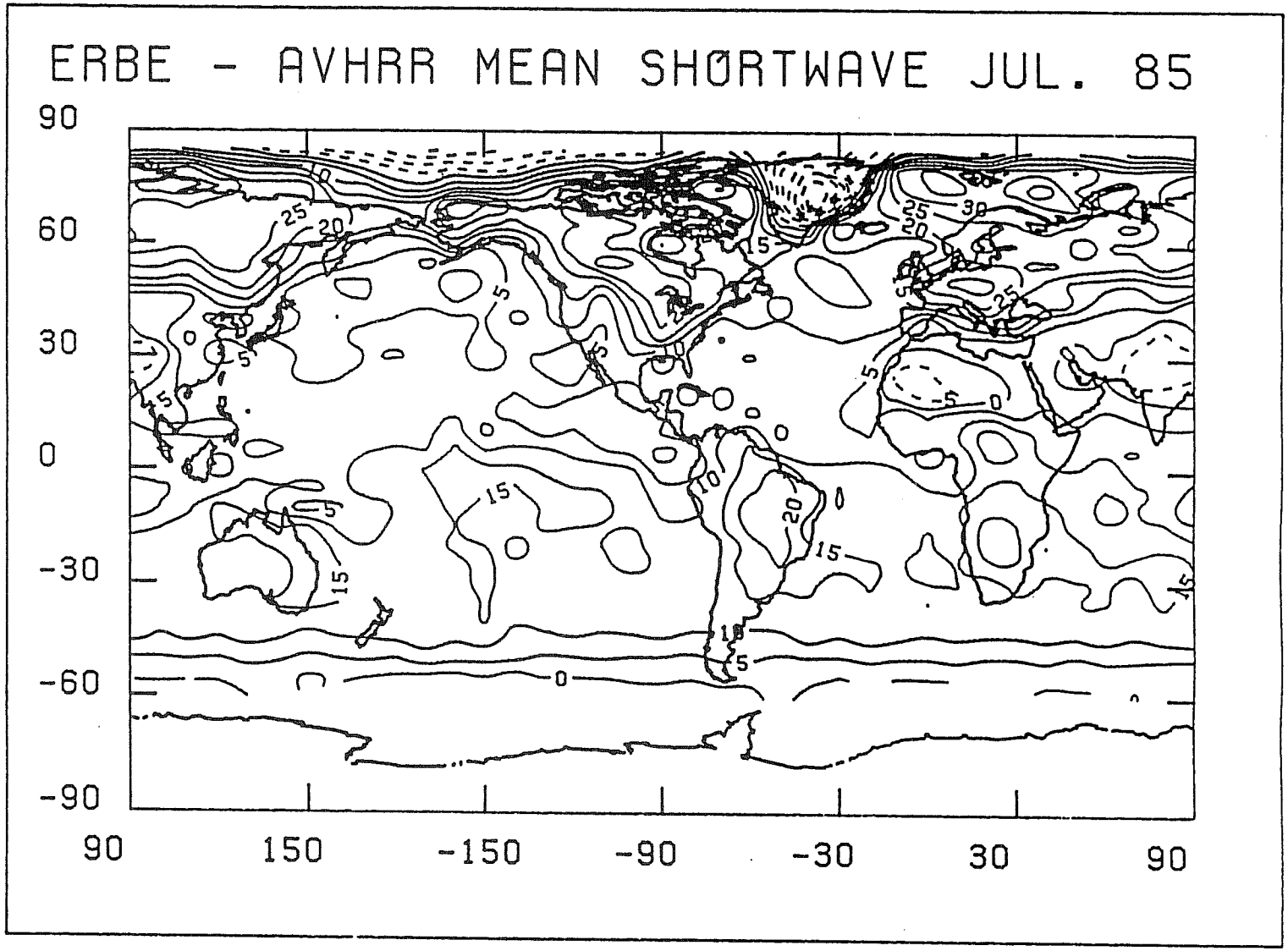

Fig. 5 Spatial distribution of shortwave difference field, (ERBE-AVHRR), in Wm^{-2} July 1985.

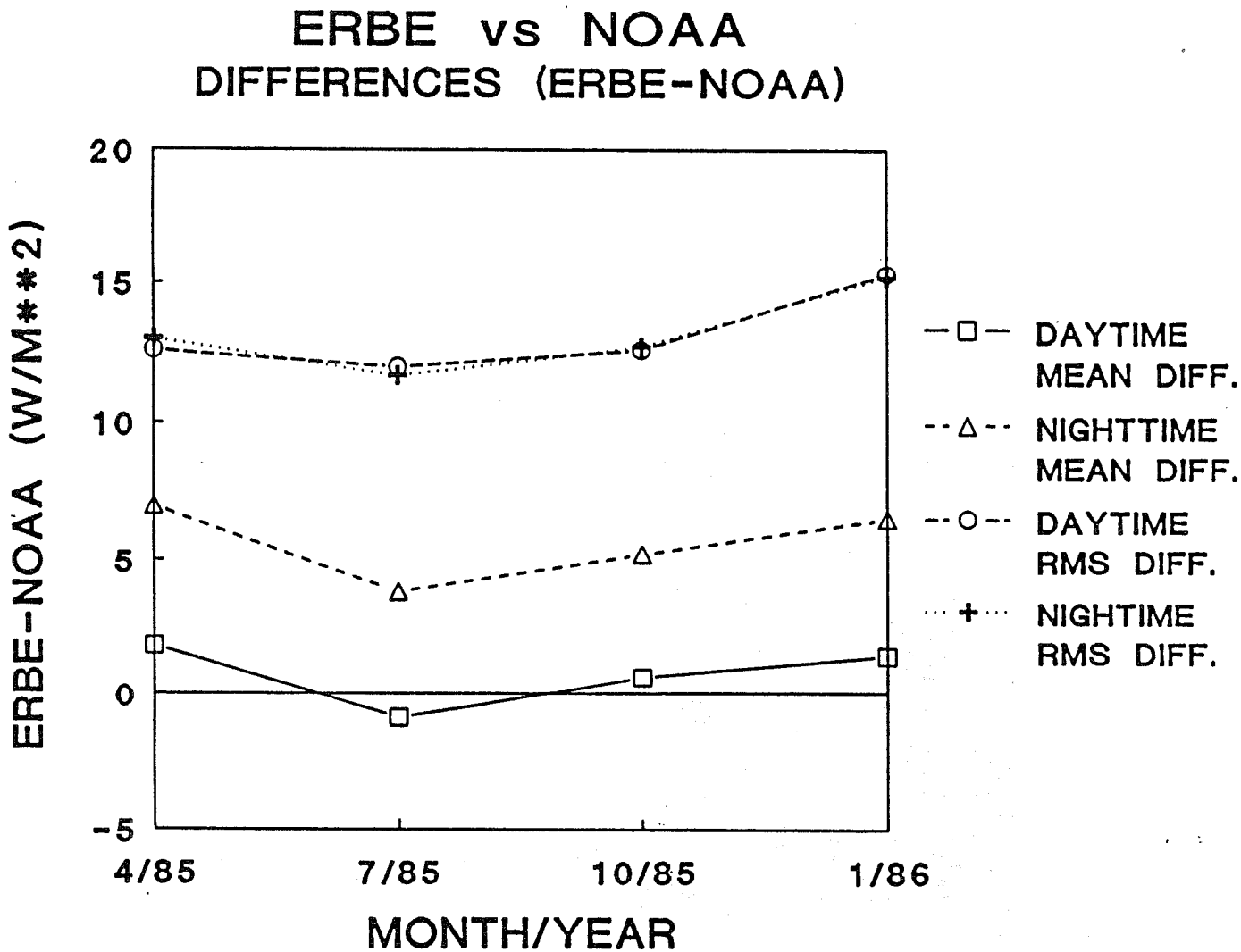

Fig. 6 A mean and RMS difference in Wm^{-2} for Daytime and nighttime OLR flux for April, July, October, 1985 and January 1986.

than broadband albedos over clouds, snow and deserts, about equal to water albedo and less than vegetated surface albedo (Laszlo et al., 1988). Since clouds are ubiquitous one might expect that, on average, the AVHRR albedo to be greater than the ERBE albedo. The fact that they are not suggests the importance of bi-directional and directional models and the lack of onboard calibration. These individual factors need to be isolated and studied.

Nevertheless, there is information about the planetary albedo that can perhaps be exploited. One way may be to develop empirical models between AVHRR narrowband data and collocated ERBE data as done, for example, by Jacobowitz and Gruber (1990).

3.2 Outgoing longwave radiation

Most of the results in this section were adapted from previous work by Gruber et al. (1990). A global comparison of the RMS and mean difference (ERBE - NOAA) is shown in Figure 6. Results are shown for both day and night. The RMS difference is about 12-14 Wm^{-2} while the mean difference varies between about -1 to 2 Wm^{-2} during the daytime but is about 5-7 Wm^{-2} during the nighttime. Interestingly this difference between the day and night flux might be related to a bias noted in the ERBE scanner flown on NOAA-9 which tends to yield a longwave flux during the daytime that is about 2% too low (Green, personal communication, 1989). However, as will be seen when we discuss the regional comparisons, a significant cause of the differences between ERBE and AVHRR estimates of outgoing longwave radiation are probably related to problems associated with the inability of a window channel to adequately detect significant departures of the atmospheric moisture and temperature profiles from the average.

The linear correlation of the two data sets varies from .95 to .97, indicating a high degree of spatial agreement between the two data sets, similar to the shortwave data.

The daytime emitted longwave flux field for July 1985 as estimated by ERBE is illustrated in Figure 7a and is shown as a representative sample of the other months studied. The spatial distribution of OLR shown in this figure should be quite familiar as it has been documented numerous times beginning with the earliest space based observations such as VonderHaar and Suomi (1971) and most recently with ERBE data, (for example, Harrison et al., 1988). Briefly, there is a well defined latitudinal gradient in OLR with low values in polar latitudes and high values in the tropics and sub - tropics. The high latitudes, especially in the winter hemisphere, tends to exhibit a structure that is zonally oriented, while the tropics and subtropics exhibit more east west variability due to the distribution of deep convective cloud systems, mainly over continents, and the relatively cloud free sub-tropical high pressure zones. This pattern is fairly stable although it does vary latitudinally with the seasons. The corresponding longwave flux field as estimated by AVHRR is provided in Figure 7b. Though subtle differences are apparent, all of the salient features of the ERBE field are well replicated in pattern and magnitude.

The difference between the two daytime OLR estimates (ERBE minus AVHRR) is presented in Figure 8a. The dominant feature of this map is the set of systematic biases of from 5 to 15 Wm^{-2} present over the oceanic subtropics, where the AVHRR measurements are consistently lower than the ERBE values. A second feature worthy of note is the area of pronounced negative difference (exceeding -15 Wm^{-2}) over the Sahara Desert and northern Africa and Saudi Arabia in general, where the AVHRR estimates exceed those from ERBE. Poleward of the 30° latitudes, the agreement between the AVHRR and ERBE longwave flux estimates is generally good for this month.

The difference between the AVHRR and ERBE OLR fields at night is portrayed in Figure 8b. The nighttime differences are quite similar to those of the daytime with two notable departures. First, the differences between the two estimates are on the order of 5 Wm^{-2} greater at night than during the day; this is particularly evident over the oceans. Second,

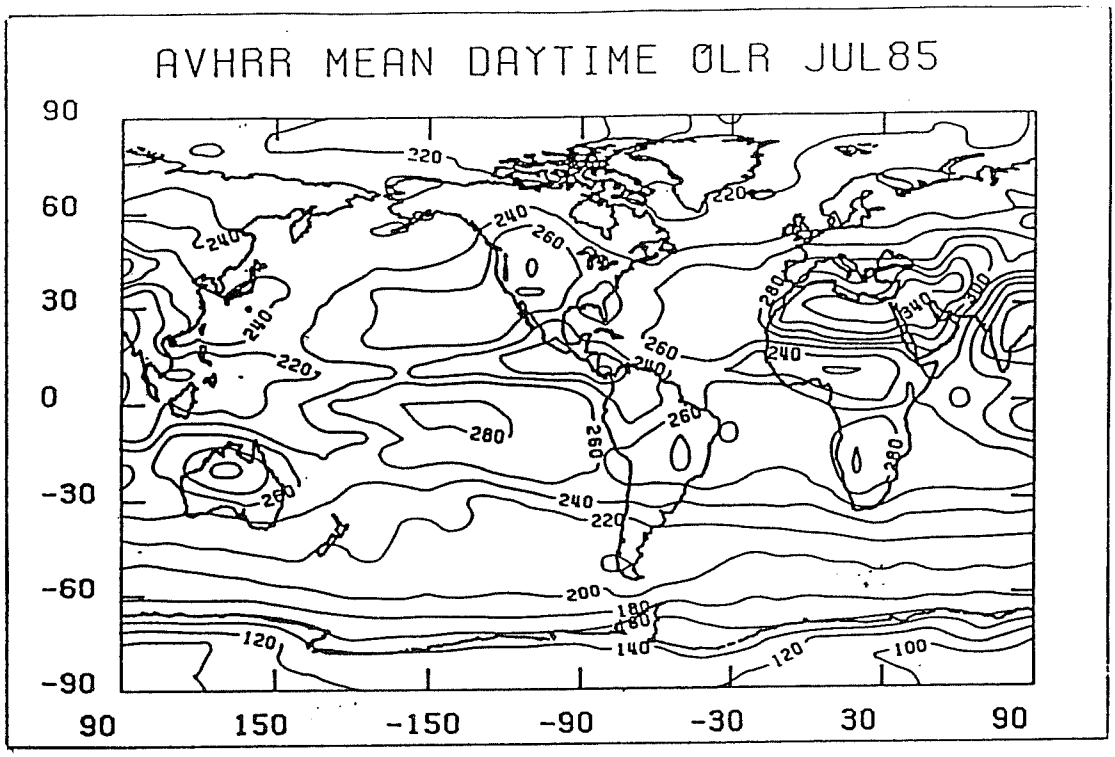

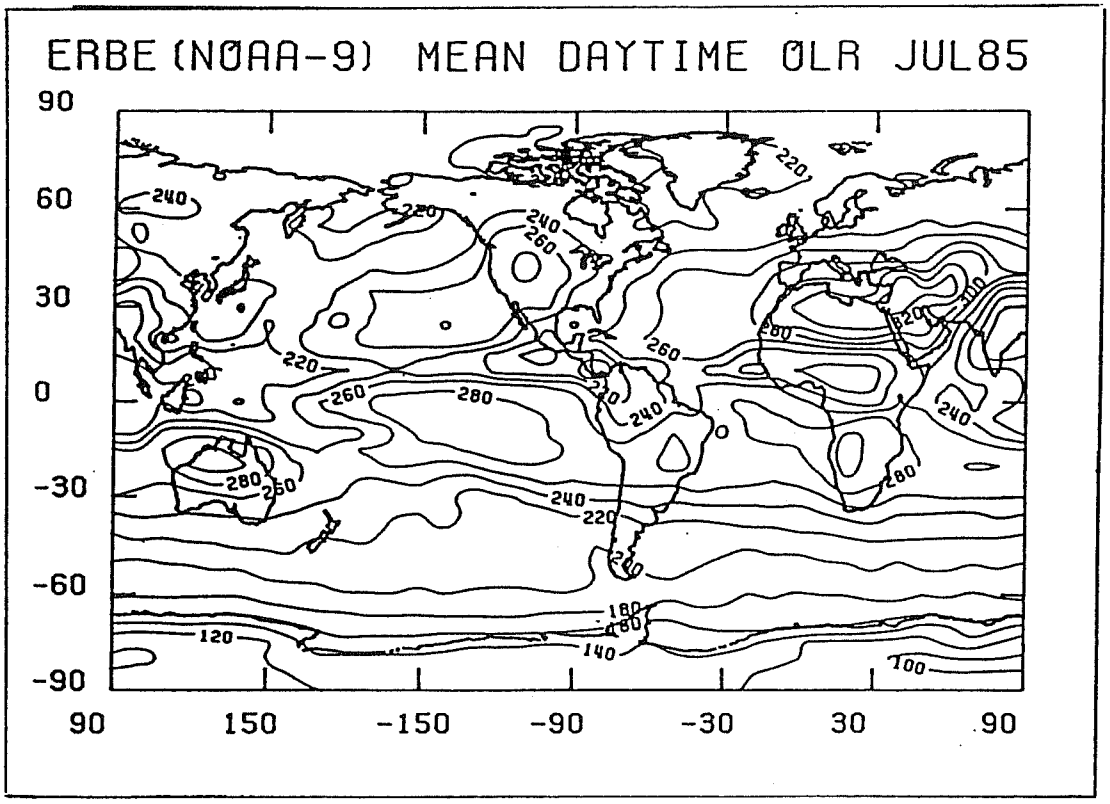

Fig. 7 Spatial distribution of daytime OLR for July 1985, Wm^{-2}.
(a) AVHRR (b) ERBE

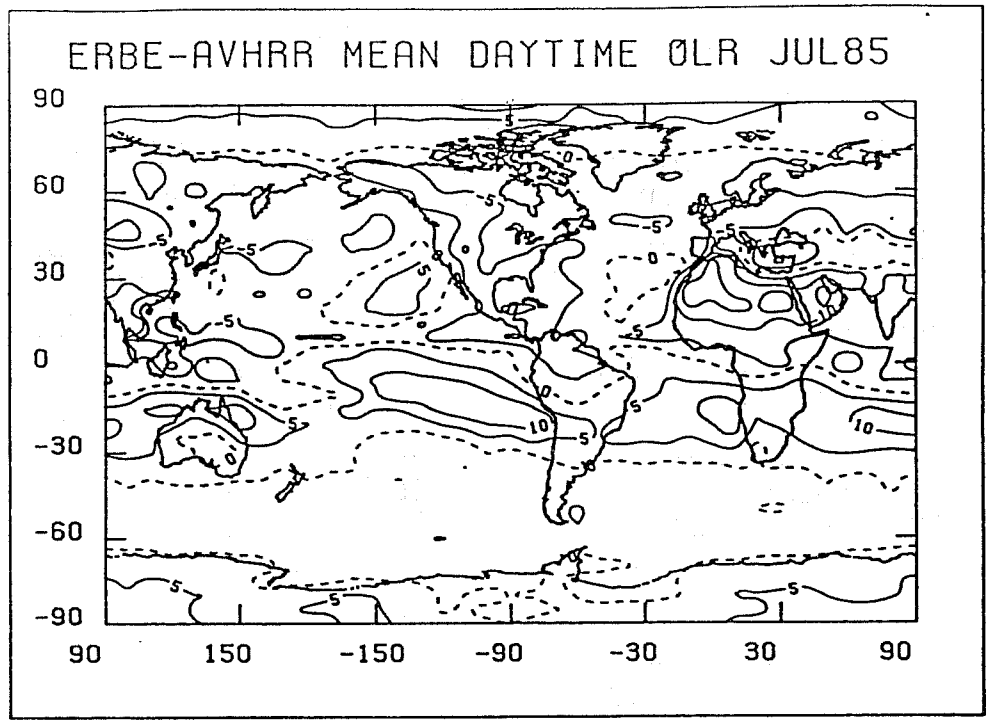

(a)

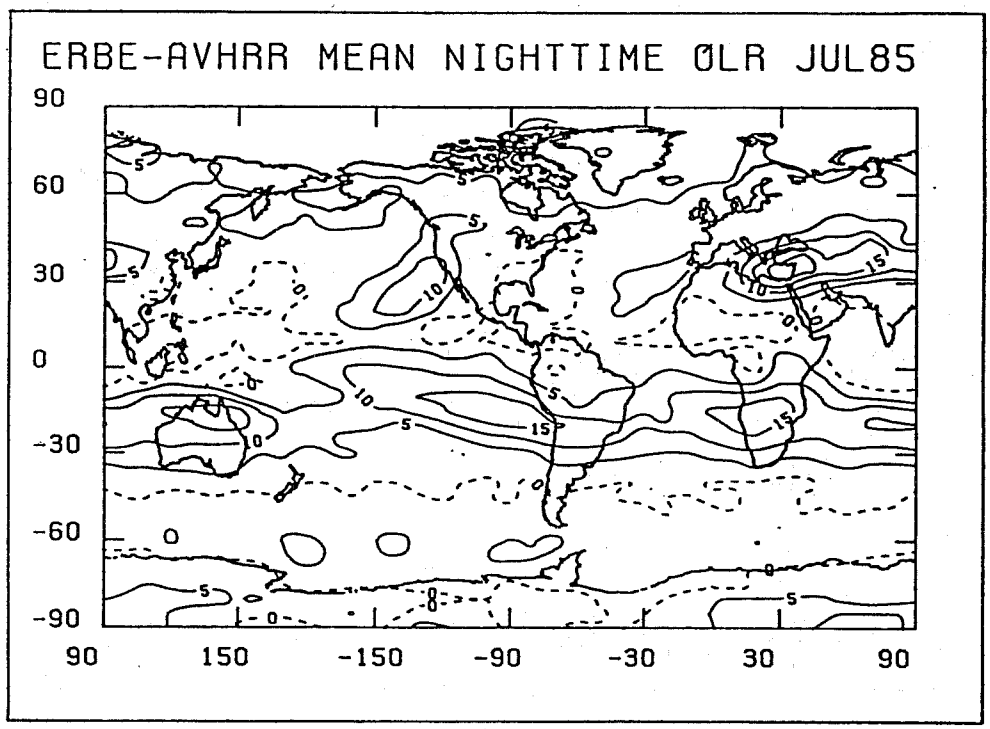

(b)

Fig. 8 Spatial distribution of OLR differences, Wm^{-2}.
(a) daytime, (b) Nightime, July 1985.

the negative difference over north Africa, and a smaller region over Australia, have vanished. Now, difference maxima are present over Africa and Australia.

The dramatic differences found over the oceanic subtropical high-pressure regions, (ERBE > AVHRR), and the daytime deserts (AVHRR > ERBE) are in areas that have persistent climatological features. Since the window channel responds primarily to surface temperature, it is reasonable to suspect that the differences are in large part driven by an inability of the AVHRR algorithm to deal with the atmospheric structure found in those areas. For example, the temperature and moisture structure in oceanic sub-tropical high pressure zones is characterized by a "trade wind" inversion (Riehl, 1979) which is strongest in the eastern ocean and weakens as one progresses westward. Desert areas experience enormous diurnal changes of soil surface temperature which can lead to corresponding large soil surface-air temperature discontinuities. Smith (1986) reports 2.5 cm soil-air temperatures discontinuities of about 25-30°C during the day and near zero or ± a few degrees Centigrade temperature discontinuity at night over a station in the Arabian Peninsula. Stowe et al. (1988), found similar results over deserts comparing skin temperature from a 10-12 μm radiometer and analyzed surface air temperatures. Since these regions are mostly cloud free or have very few clouds the single channel AVHRR algorithm may be insensitive to the variations in atmospheric moisture and temperature structure and return fluxes that are dominated by the surface temperature. Relative to a broad-band flux determination such as available from ERBE, one might expect the AVHRR to overestimate flux values over deserts during the day, be similar in magnitude to deserts during the night and underestimate the flux over the trade wind region in proportion to the strength of the inversion and moisture distribution. Interestingly, the magnitude of the ERBE-AVHRR differences over the oceans decreases as one moves westward consistent with the observed weakening of the trade wind inversion and increase in moisture.

These ideas were tested by calculating the sensitivity of the operational single-channel algorithm to variations of temperature structure over deserts and temperature and water vapor structure in the trade-wind region. Each will be described below.

3.2.1 Desert Areas

For the desert areas a set of observed atmospheric soundings (pressure, temperature, and dewpoint depression) were collected from various desert locations (Texas, Egypt, Algeria and Nigeria). The soundings were separated into daytime and nighttime, and longwave fluxes were calculated using the model described by Ellingson et al. (1989a) and comparisons were made to OLR estimated from the AVHRR 11 μm channel. The calculated broad-band OLR was taken as "truth." Calculations were made based on the soundings as given and for various temperature discontinuities between the surface skin temperature and air temperature. For the day (night) soundings temperature discontinuities of +1 (-1), +3 (-3), +5 (-5), +10 (-10), +15 (-15), and +20 (-20)°C were tested.

The results of the calculations are shown in Figure 9. The variation is nearly linear over the range of temperature calculated, with a slightly different slope during nighttime hours. The important point to note is that the magnitudes of the differences are consistent with the observed differences between ERBE and AVHRR and is also supported by the skin-air temperature differences reported by Smith (1986) and Stowe et al. (1988). This is clearly a situation where a window channel algorithm is inadequate.

3.2.2 Trade-Wind Region

The calculations for the trade wind region were performed for a typical trade wind sounding taken from Riehl (1979). The strength of the inversion was modified from +2 to -10°C at each level by 2°C increments. The water content was held fixed. The results are summarized in Figure 10. The results

DESERT SIMULATIONS

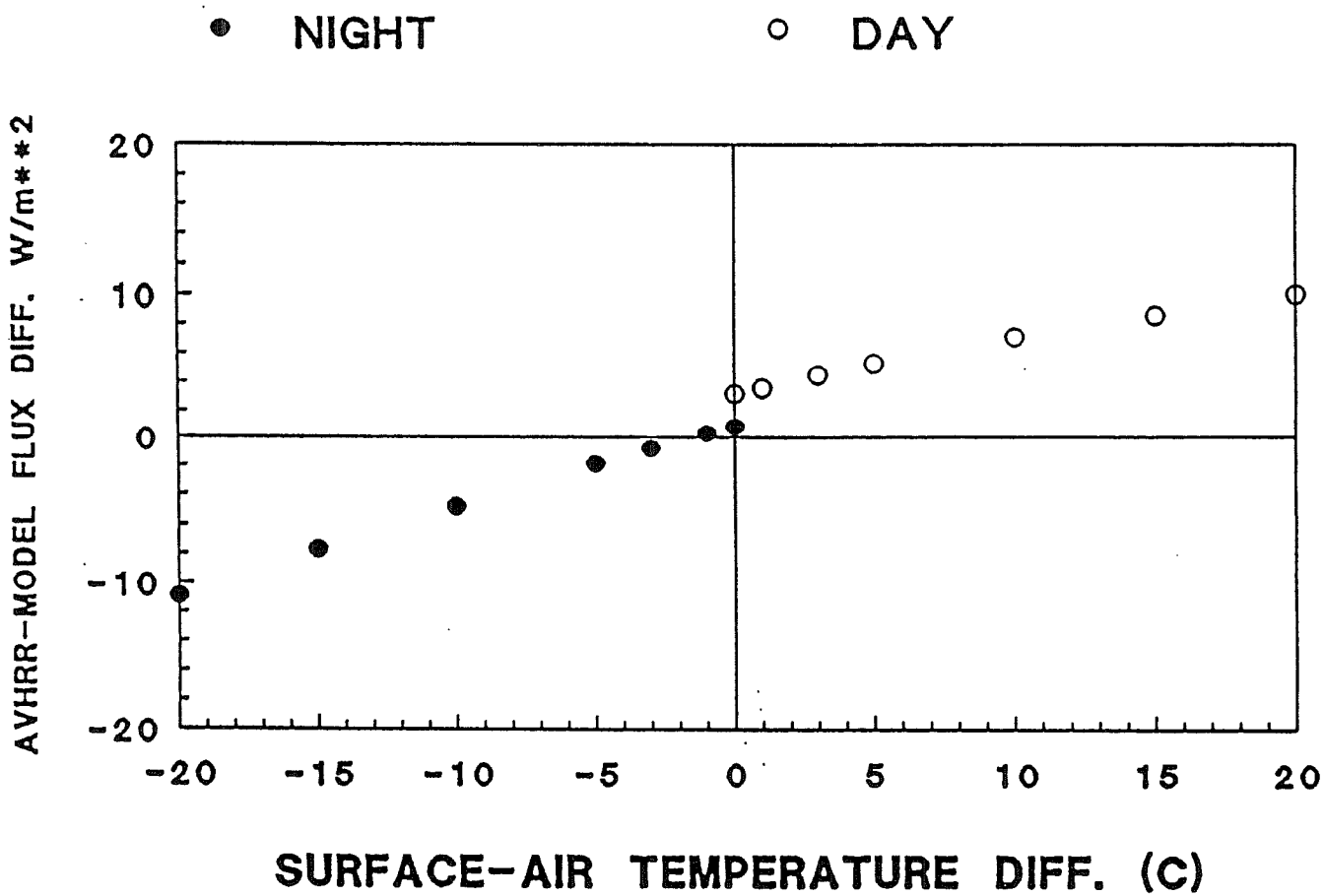

Fig. 9 Simulations of skin - air temperature impact on OLR for observed desert soundings.

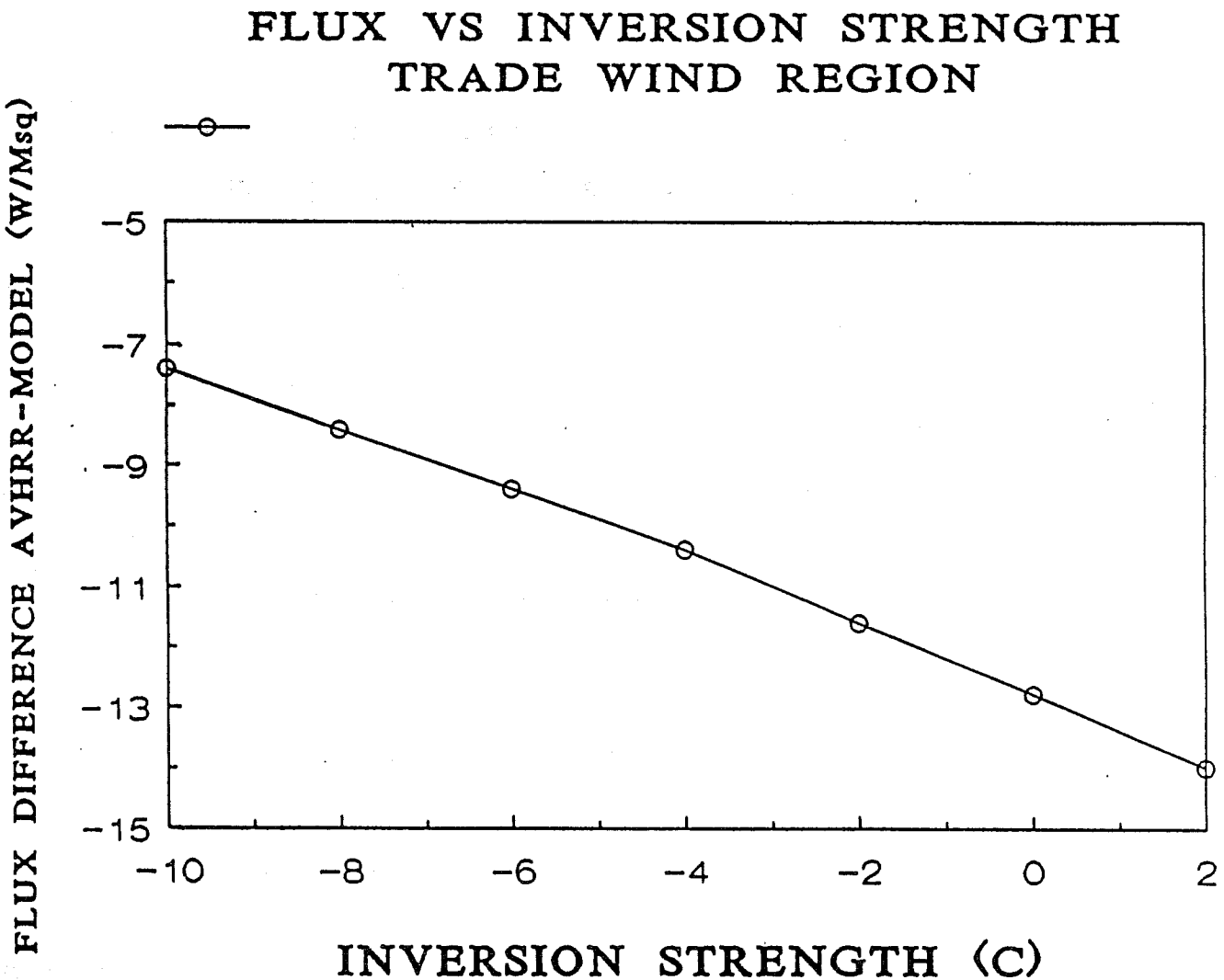

Fig. 10 Simulation of the variations in OLR with strength of the trade wind inversion. Strength 0 is the normal trade wind sounding given by Riehl.

show AVHRR estimated flux less than modeled flux by 14 Wm^{-2} to about 8 Wm^{-2} depending on inversion strength.

A simulation was also performed to test the sensitivity of the calculations to variations in water vapor, which increase from east to west along the trade wind inversion. For an increase of precipitable water from about 2 to 3 cm (Riehl, 1979), we can expect the difference between AVHRR and ERBE to decrease by about 5 Wm^{-2} mainly due to a decrease in ERBE flux with hardly any decrease in AVHRR.

Thus, not only will the weakening trade-wind inversion lead to smaller differences between AVHRR and ERBE, but so will the variation of water vapor. The results of both temperature and moisture simulations support the view that the cause of the systematic error observed in the tropical oceans is the inability of the window channel algorithm to respond to the unique and persistent temperature and moisture structure present in the trade-wind region.

3.3 Improvements to the OLR

New algorithms using the HIRS sounding instrument of TOVS have been developed which has essentially eliminated the bias resulting from the insensitivity of the window channel to the conditions described above. This new algorithm (Ellingson et al., 1989b) utilizes a linear combination of 4 HIRS channels (13.1 - 13.6 μm, 7.9 - 8.5 μm, 6.6 - 6.9 μm and 14.3 - 14.7μm) which are sensitive to the temperature and moisture structure of the atmosphere. Results of comparisons against ERBE targets (Ellingson, 1990), shown in Figure 11, indicate considerably reduced biases, over specific surface types and greatly reduced RMS differences ($\approx$ 4 wm^{-2} for all surfaces combined). We are planning to implement this algorithm in the NOAA K,L,M processing system and would like to use this algorithm should HIRS data be re-processed.

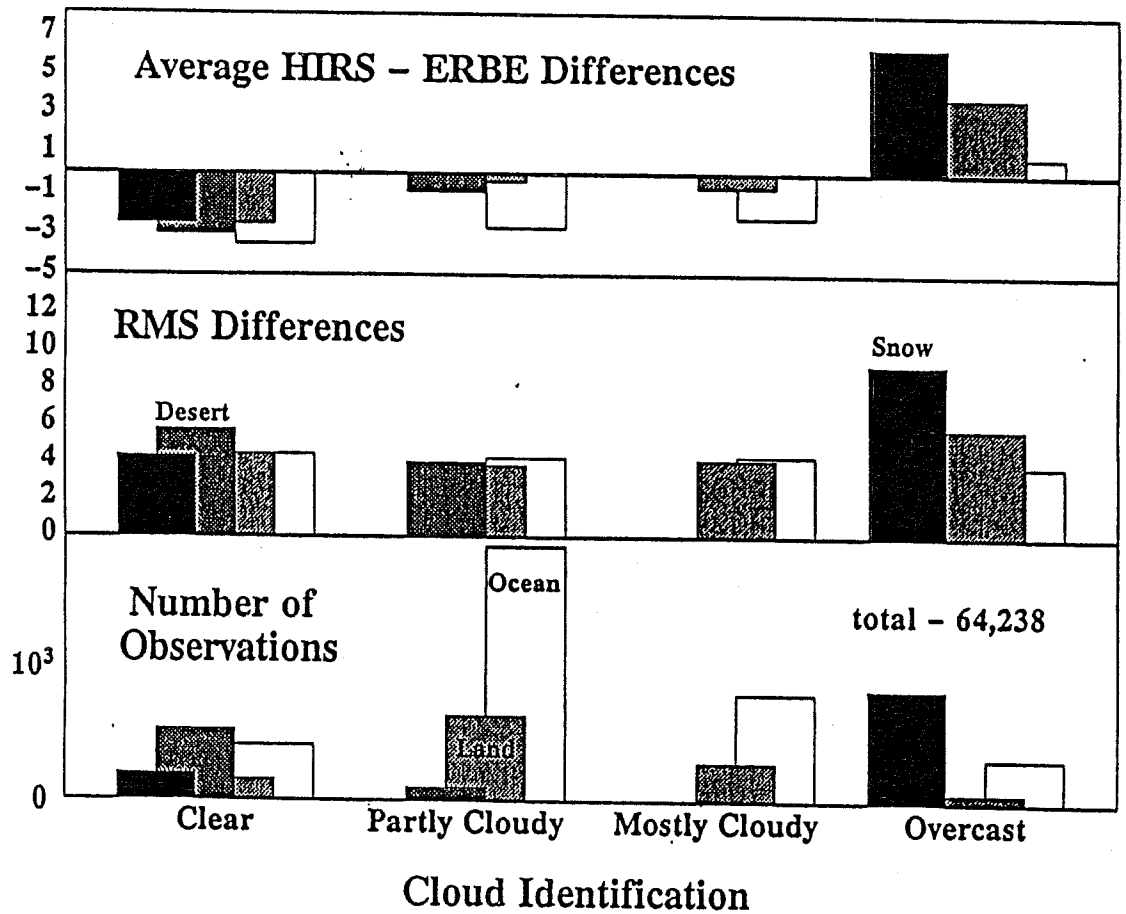

Fig. 11 A comparison of HIRS and ERBE longwave fluxes for various scene types and cloud conditions for April 1985.

4. LONGWAVE CLOUD FORCING ANOMALIES

Most of the material in this section summarizes previously presented work by Gruber and Thomasell (1990) and is being repeated here to emphasize an application of the NOAA OLR data set to the study of cloud radiation interactions.

Ramanathan (1987), has shown that by calculating the difference between the cloud free and cloudy fluxes, one can obtain a measure of the radiative effects of clouds. This quantity, called cloud forcing, is expressed as

$$CF = F_{clr} - F_{cld} \tag{3}$$

where F_{clr} is the clear longwave flux and F_{cld} is the cloudy longwave flux. A similar expression can be written for the shortwave flux, but only the longwave cloud forcing will be considered here. As discussed by Gruber and Thomasell (1990) the cloud forcing anomaly equals the anomaly in the clear flux minus the anomaly in the average or cloudy flux (Eq. 4)

$$\begin{aligned} CF' &= CF - \overline{CF} \\ CF' &= F'_{clr} - F'_{cld} \end{aligned} \tag{4}$$

where $(\bar{x})$ is the time average and $(x)'$ is the departure. They showed that it was possible to make an estimate of the cloud forcing anomaly from readily available OLR anomalies calculated from the NOAA OLR data set (Gruber et al., 1986) and the surface temperature anomaly field. Surface temperature anomalies were used to estimate the clear flux anomaly since it is not possible to obtain accurate clear fluxes from the 2.5^0 latitude / longitude grid (Gruber and Stowe, 1989). It was assumed that the clear flux anomaly was given by

$$F'_{clr} = T'_{SFC} \; X \; \partial F/\partial T_{SFC} \qquad (5)$$

and a value of 2 Wm^{-2} was used for $\partial F/\partial T_{SFC}$, based on work reported by Ohring and Gruber (1983). Surface temperature anomalies were taken from Jones et al. (1986) for the land areas and Reynolds(1986) for the ocean areas. Anomalies were calculated from 30S to 60N. Figures 12 a, b show the distribution of OLR and clear flux anomalies, respectively, for February 1983, which was near the peak El Niño which is clearly delineated by the extraordinarily large OLR anomalies in the tropical Pacific and Indian Ocean. Comparison of the two fields clearly shows that the OLR anomaly in the tropics is about an order of magnitude larger than the clear flux anomaly, clearly the result of large anomalies in cloudiness. This of course means that the pattern of cloud forcing anomaly, as shown in figure 13, will look much like the pattern in OLR anomaly.

In the mid-latitudes the clear and OLR anomaly are about the same order of magnitude, and over central Asia and North America the clear and cloudy anomalies are the same sign. This will result in cloud forcing anomalies that are small or zero as shown in Figure 13.

Only the longwave component of the cloud forcing anomaly has been shown. Over the tropical pacific the anomalies are due mainly to changes in cloudiness which undoubtedly have associated changes in albedo. It is likely that there would be negative (positive) shortwave cloud forcing thus tending to cancel the positive (negative) longwave cloud forcing. However, the longwave forcing mainly goes to heating or cooling the atmosphere while the shortwave forcing mainly affects the surface. Thus, the large positive cloud forcing anomaly associated with El Nino will act to enhance any warming due to surface temperature rise or latent heat release. Gruber and Thomasell estimated that the longwave

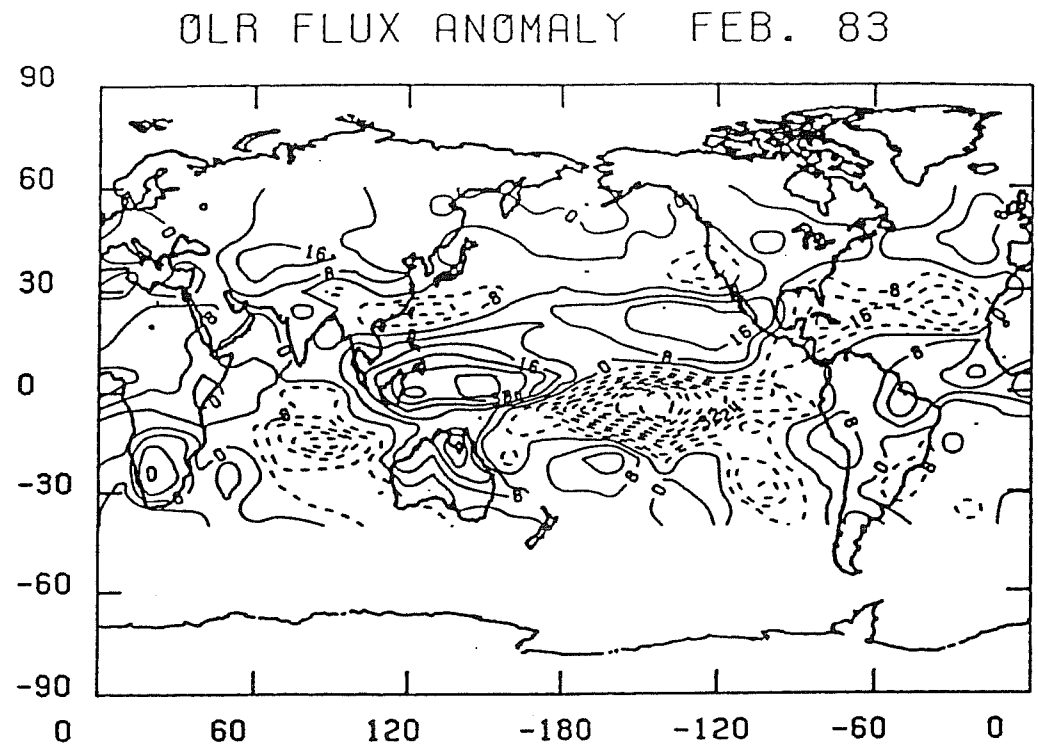

(a)

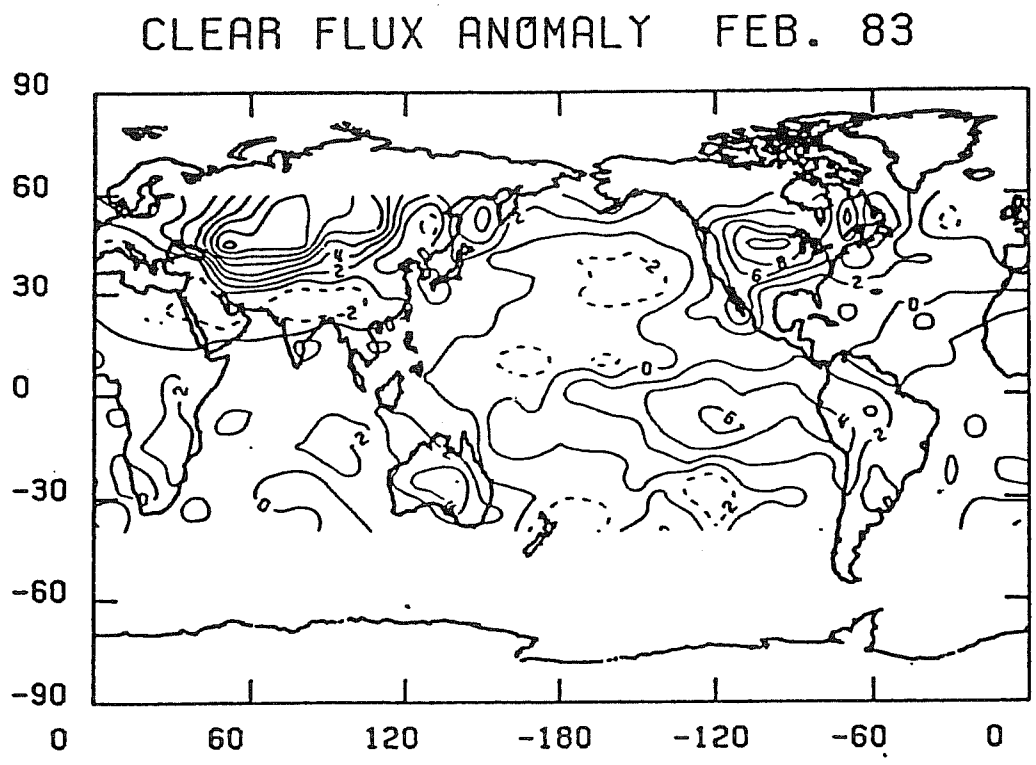

(b)

Fig. 12 Spatial distribution of flux anomaly in Wm^{-2}, (a) OLR flux anomaly, (b) clear flux anomaly, February, 1983.

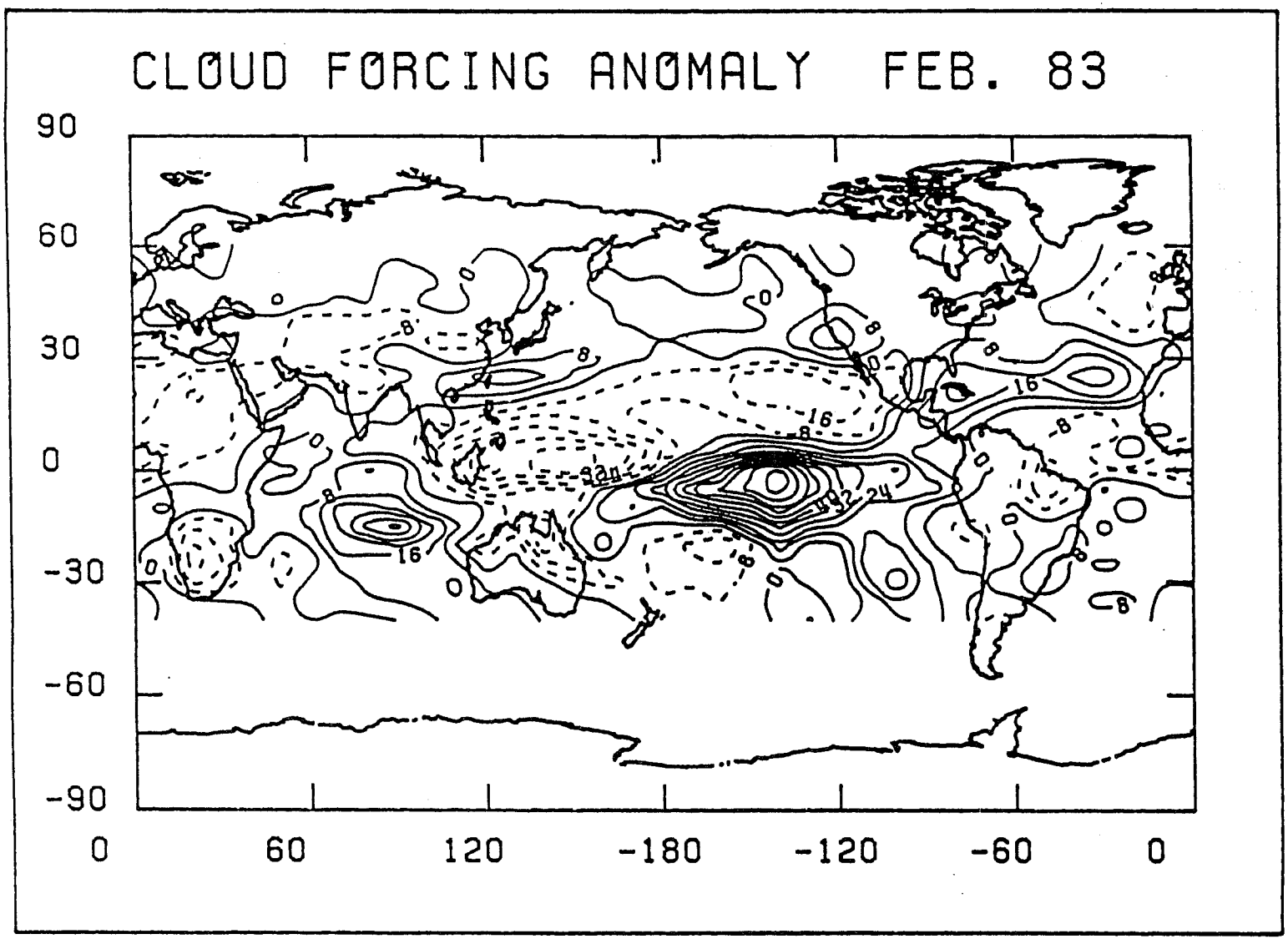

Fig. 13 Spatial distribution of the cloud forcing anomaly, February, 1983.

heating of the large positive anomaly was about 0.8C/day and was about 1/3 of the anomalous latent heating. This is not an insignificant quantity, and should be accounted for in climate models. We are in the process of preparing estimates of longwave cloud forcing for the record of OLR data, for the period June, 1974 through December 1984.

5. REFERENCES

Abel, P. and A. Gruber, 1979: An improved model for calculation of longwave flux at 11μm. NOAA Tech. Memo. NESS 106, NOAA, Wash., D. C., 24pp.

Barkstrom, B. R., E. F. Harrison, G. L. Smith, R. D. Cess, the ERBE Science Team, and the ERBE Data Management Team, 1988: Earth Radiation Budget Experiment (ERBE) Validation, Archival, and April 1985 Results, Bull. Amer. Meteor. Soc., In press.

Brest, C. L. and W. R. Rossow, 1990: Radiometric calibration and modeling of NOAA AVHRR data for ISCCP. Int. J. Rem. Sensing , in press

Ellingson, R., 1990: Personal communication.

Ellingson, R.E., D.J. Yanuck and A. Gruber, 1989a: On the effects of the choice of meteorological data on radiation model simulation of the NOAA technique for estimating outgoing longwave radiation from satellite radiance observations. J. Clim., 2, 761-765.

Ellingson, R.E., D.J. Yanuck, H.T. Lee and A. Gruber, 1989b: A technique for estimating outgoing longwave radiation from HIRS radiance observations. J. Ocean, Atmos. Techn., 6, 706-711.

Green, R. 1989: Personal communication.

Gruber, A., 1977: Determination of the Earth - atmosphere radiation budget from NOAA satellite data. NOAA technical Report NESS 76, U.S. Department of Commerce, Washington D.C. 28pp.

Gruber, A., and A. F. Kruger, 1984: The status of the NOAA outgoing longwave radiation data set. Bull. Am. Meteorol. Soc., 65, 958-962.

Gruber, A., M. Varnodore, P.A. Arkin, J.S. Winston, 1986: Monthly and seasonal mean outgoing longwave radiation and anomalies. NOAA Tech. Rpt., NESDIS 26.

Gruber, A. and L.L. Stowe, 1989: An analysis of cloud radiation forcing as calculated from ERBE, AVHRR and Nimbus-7 ERB and cloud data. Adv. Space Res., 9, (7) 129 - (7) 138.

Gruber, A. R. Ellingson, S. Oh, P. Ardanuy, M. Weiss and S. K. Yang, 1990: A comparison of AVHRR and ERBE longwave radiation estimates. Preprint Vol. of Fifth Conf. on Sat. Meteor. and Ocean., Sept 3-7, London, Eng., Amer. Meteor. Soc., 50-54.

Gruber, A. and A. Thomasell, 1990: Cloud radiative forcing obtained from NOAA OLR data. Preprint Vol of the Symp.on Global Change Systems and the Spec. Sessionns onClim. Var. and Hydrol.,Feb. 5-9,1990, Anaheim, Cal., Amer. Meteor. Soc., 146-148.

Harrison, E. F., D. R. Brooks, P. Minnis. B. R. Wielicki, W. F. Staylor, G. G. Gibson, D.F. Young, F. M. Denn and the ERBE Science Team, 1988: First estimates of the diurnal variation of longwave radiation from the multiple-satellite Earth Radiation Budget Experiment (ERBE). Bull. Amer. Meteor. Soc., 69, 1144-1151.

Jacobowitz, H. and A. Gruber, 1990: Estimation of the broadband planetary albedo from narrowband NOAA satellite observations. Preprint vol of the Seventh Conf.on Atmos. Rad., July 23-27,1990. Amer. Meteor. Soc., 161-163.

Jones, P.D., S.L.B. Roper, R.S. Bradley, H.F. Diaz, P.M. Kelly and T.M.L. Wigley, 1986: Northern hemisphere surface air temperature variations: 1851-1984. J. Clim. Appl. Meteor., 25, 161-179.

Laszlo, I., H. Jacobowitz. and A. Gruber, 1988: The relative merits of narrowband channels for estimating broadband albedos. J. Atmos. and Ocean. Techn., 5,757-773.

Ohring, G. and A. Gruber, 1983: Satellite Radiation Observations and Climate Theory. Advances in Geophysics, 25, 237-304.

Ohring, G., A. Gruber and R. Ellingson, 1984 Satellite determination of the relationship between total longwave radiation flux and infrared window radiance. J. Clim. Appl. Meteor., 23, 416-425.

Ramanathan, V., 1987: The role of Earth radiation budget studies in climate and general circulation research. J. Geophys. Res., 92, 4075-4095.

Reynolds, R.W., 1988: A real time global sea surface temperature analysis. J. Clim., 1, 75-86.

Riehl, H., 1979: Climate and Weather in the Tropics, Academic Press, 611 pp.

Smith, E.A., 1986: The structure of the Arabian heat low. Part I: Surface energy budget. Mo. Wea. Rev., 114, 1067-1083.

Staylor, F. W. 1990: Degradation rates of the AVHRR visible channel for the NOAA 6, 7, and spacecraft. J. Atmos. and Ocean. Technology, 7, 411-423.

Stowe, L.L., C.G. Wellemeyer, T.F. Eck, H.Y.M. Yeh and the Nimbus-7 Cloud Data Processing Team, 1988: Nimbus-7 Global Cloud Climatology. Part I: Algorithms and Validation. J. Clim., 1, 445-470.

Taylor, V. R., 1990: Implementation of reflectance models in operational AVHRR radiation budget processing. NOAA Technical Rpt NESDIS 49, NOAA, Washington D. C., 20pp.

Taylor, V. R., and L. L. Stowe, 1984: Reflectance characteristics of uniform Earth and cloud surfaces derived from Nimbus-7 ERB. J. Geophs. Res., 89, 4987-4996.

Vonder Haar, T. H. and V. E. Suomi, 1971: Measurements of the Earth's radiation budget from satellites during a five year period. Part 1: Extended time and space means. J. Atmos. Sci., 28, 305-314.